2021 CERN Summer Student Project Report

Search for the doubly charmed baryon Ξ_{cc}^{+} at LHCb

Student: Danyi Zhang[1]
Supervisors: Jibo He[1], Monica Pepe-Altarelli[2]

[1] *University of Chinese Academy of Sciences, Beijing, China*
[2] *European Organization for Nuclear Research (CERN), Geneva, Switzerland*

Abstract

The search for the doubly charmed baryon Ξ_{cc}^{+} decay to $\Lambda_c^+ K^- \pi^+$ is re-optimized on the basis of a previous study based on Run 1 and Run 2 data. We perform a preliminary study of the event selection and background in the new decay mode $\Xi_{cc}^{+} \rightarrow \Xi_c^0 \pi^+$ using Run 2 data.

Contents

1 Introduction

1.1 Doubly charmed baryon at LHCb

The Ξ_{cc}^{+} baryon is one of the ground states of the doubly charmed baryons. Unlike a conventional baryon such as the proton, the doubly charmed baryon contains two heavy quarks, and provides a unique system for testing quantum chromodynamics (QCD). Doubly charmed baryons are expected to have a sizable production cross-section at hadron colliders [1–4].

In 2017, the LHCb collaboration [5], reported the observation of a highly significant structure in the invariant mass of $\Lambda_c^+ K^- \pi^+ \pi^+$, consistent with the Ξ_{cc}^{++} baryon. The measured mass is $M_{\Xi_{cc}^{++}} = 3621.40 \pm 0.72\,(\text{stat}) \pm 0.27\,(\text{syst}) \pm 0.14\,(\Lambda_c^+)\,\text{MeV}/c^2$, which differs by $103 \pm 2\,\text{MeV}/c^2$ from that of the isospin partner, the Ξ_{cc}^{+} baryon, measured by the SELEX collaboration [6]. This difference is much larger than that expected from isospin splitting, which is usually a few MeV/c^2. The observation of the Ξ_{cc}^{++} baryon was confirmed by LHCb in the decay mode $\Xi_c^+ \pi^+$ [7], giving a measured mass of $3620.6 \pm 1.5\,(\text{stat}) \pm 0.5\,(\text{syst})\,\text{MeV}/c^2$, which is consistent with the previous measurement.

The subsequent measurement of the Ξ_{cc}^{++} lifetime of $0.256\,^{+0.024}_{-0.022}\,(\text{stat}) \pm 0.014\,(\text{syst})$ ps [8] established the weakly decaying nature of the Ξ_{cc}^{++} baryon. Theoretical models predict that the lifetime of the Ξ_{cc}^{+} should be shorter by a factor of 3 than that of its isospin partner, the Ξ_{cc}^{++}, thus predicting a lifetime of 80 fs. A recent study searching for the Ξ_{cc}^{+} in the decay $\Lambda_c^+ K^- \pi^+$ at LHCb reported the largest local significance of 3.1 standard deviations at around $3620\,\text{MeV}/c^2$. [9]. The background-subtracted decay time distribution of the Ξ_{cc}^{+} was also checked, indicating that $\tau(\Xi_{cc}^{+})$ is likely to be around 45 fs. The Ξ_{cc}^{+} baryon was also searched in the decay mode $\Xi_{cc}^{+} \to \Xi_c^+ \pi^+ \pi^-$, which was then combined with the search for $\Xi_{cc}^{+} \to \Lambda_c^+ K^- \pi^+$, leading to a local significance of 4.2 standard deviations [10].

1.2 Motivation

Based on the previous searches for the Ξ_{cc}^{+} baryon, this work is intended to re-optimize the event selection of the decay $\Xi_{cc}^{+} \to \Lambda_c^+ K^- \pi^+$ and take a first look at the new decay mode $\Xi_{cc}^{+} \to \Xi_c^0 \pi^+$.

For the $\Xi_{cc}^{+} \to \Lambda_c^+ K^- \pi^+$ decay, there are at least three aspects that could be improved from the previous study. The Ξ_{cc}^{+} candidates are selected from the exclusive Turboline, which has a low efficiency for the K^- and π^+ selection, as shown in Table 1. Secondly, according to the theory predictions and the LHCb internal result, the lifetime of Ξ_{cc}^{+} could be smaller than 80 fs. The decay time distribution of the Ξ_{cc}^{+} in Fig. 1 and Fig. 2 from the internal note show that the lifetime is most likely to be around 45 fs. The MVA performance could be improved by re-weighting the Ξ_{cc}^{+} lifetime from 80 to 45 fs. Also, the MVA training input variables could be improved by adding PID variables.

The $\Xi_{cc}^{+} \to \Xi_c^0 \pi^+$ decay was searched by the BaBar [11] and Belle [12] experiments without finding any evidence. The branching ratio of this process is predicted to be smaller than the already observed $\Xi_{cc}^{++} \to \Xi_c^+ \pi^+$, due to the expected shorter lifetime of Ξ_{cc}^{+} [13]. One possible Feynman diagram is shown in Fig. 3.

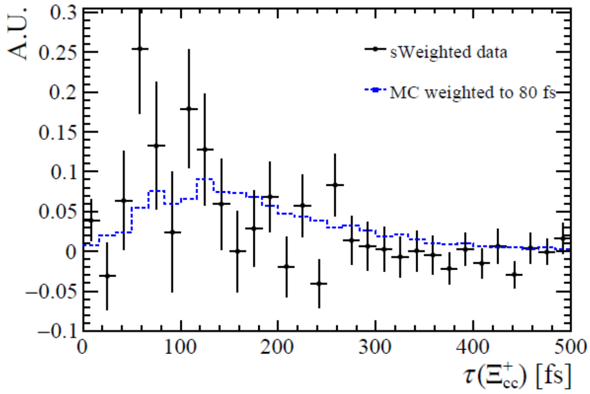

Figure 1: A comparison of the simulated and the background-subtracted decay time distribution.

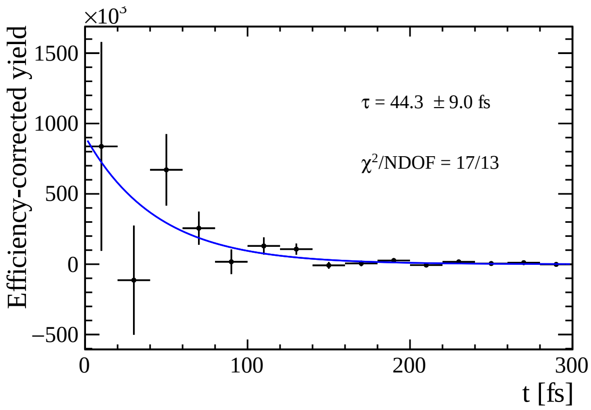

Figure 2: Efficiency-corrected background-subtracted decay time distribution, along with a fit with an exponential function.

Table 1: Part of the Turbo line selection efficiency of the $\Xi_c^+ \to \Lambda_c^+ K^- \pi^+$ decay.

Particle	Selection	Events	Efficiency
	......		
	Kaon p_{T} >500	18251	(88.98 ± 0.22)%
	Pion p_{T} >500	13440	(73.64 ± 0.33)%
Ξ_{cc}^+ daughters	Kaon particle ID DLL$_{KK}$ >10	11797	(87.78 ± 0.28)%
	Pion particle ID DLL$_{\pi K}$ <0	10620	(90.02 ± 0.28)%
	......		

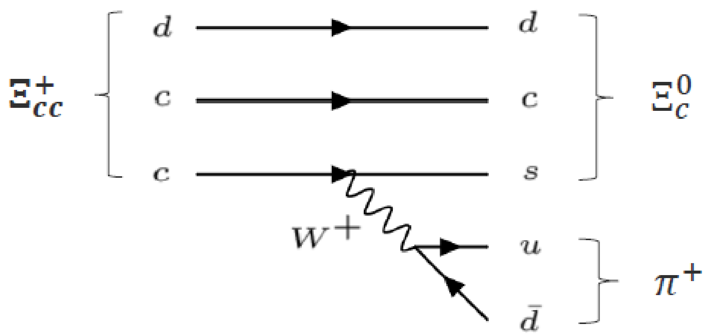

Figure 3: One possible Feynman diagram for the process of $\Xi_{cc}^{+} \to \Xi_{c}^{0}\pi^{+}$.

2 Analysis strategy

This work searches for Ξ_{cc}^{+} with both $\Xi_{cc}^{+} \to \Lambda_c^+ K^- \pi^+$ and $\Xi_{cc}^{+} \to \Xi_c^0 \pi^+$ decays, with the signal region defined as $3.3 < m(\Xi_{cc}^{+}) < 3.8\,\mathrm{GeV}/c^2$.

In the $\Lambda_c^+ K^- \pi^+$ decay, the Λ_c^+ candidate is reconstructed from the $pK^-\pi^+$ final state. As an optimization from the previous study, the Ξ_{cc}^{+} mass signal region in real data is unlinded after event selection, making it possible to roughly examine the signal significance by scanning the p-value in the signal region. Firstly, the Ξ_{cc}^{+} candidates are reconstructed at the trigger level (Turbo) in a different way from the previous study. Instead of using an exclusive Turbo line in which the p_{T} cuts on the K^- and π^+ from the Ξ_{cc}^{+} decay are too tight, Ξ_{cc}^{+} candidate is reconstructed by combining Λ_c^+ candidate in an inclusive line with K^- and π^+ selected with relaxed cuts. In order to enhance the similarity between the Monte Carlo (MC) simulation samples and the real data, MC samples are corrected based on PID calibration data, using the PID resampling tool `PIDGen`. According to previous studies, the lifetime of Ξ_{cc}^{+} is very likely to be smaller than 50 fs. Therefore, the lifetime is re-weighted in MC samples to 45 fs for studies of the nominal lifetime hypothesis. Then the multivariate selection (MVA) is introduced to optimize the signal significance. The training variables are updated adding the corrected PID variables. The cut value is determined by optimizing the sensitivity. After removing the clone and duplicated candidates, the signal shape is studied with simulated events. Finally, the signal and background are fitted under different mass hypothesis, giving the local p-value scan result.

For $\Xi_{cc}^{+} \to \Xi_c^0 \pi^+$, the search is performed in a blind manner. The strategy is similar to that of the $\Lambda_c^+ K^- \pi^+$ decay. A preliminary study of the event selection and background is performed.

3 Data and MC samples

Data collected in 2011, 2012, 2015, 2016, 2017, and 2018 are used in this analysis. For $\Lambda_c^+ K^- \pi^+$ decay, candidates are composed of inclusively reconstructed Λ_c^+ in the second level of high level trigger, combined with K^- and π^+. These data sets are referred to as right-sign (RS) samples, while the wrong-sign (WS) dataset for this decay mode is $\Xi_{cc}^+ \to \Lambda_c^+ K^- \pi^-$. For $\Xi_{cc}^+ \to \Xi_c^0 \pi^+$ decay, candidates are similarly reconstructed with inclusive Λ_c^+ in the Turboline and π^+. The WS is reconstructed with Λ_c^+ and π^-.

A dedicated generator, GenXicc2.0, is used to simulate doubly charmed baryon production [14]. To develop the selection sequences as well as efficiency studies, signal samples with different mass and lifetime configurations are generated, as summarized in Table 2.

Table 2: MC samples of Ξ_{cc}^+ with different mass and lifetime configurations.

EventType	m [MeV/c^2]	τ [fs]	Λ_c^+ decay model	Condition
26265052	3621.4	80	Pseudo-resonant	2017 Sim09f
26265052	3621.4	80	Pseudo-resonant	2018 Sim09f

4 Optimization of $\Xi_{cc}^{+} \to \Lambda_c^+ K^- \pi^+$

4.1 PID correction

In order to enhance the similarity between the MC simulation samples and the real data, MC samples are corrected based on PID calibration data, using the PID resampling tool `PIDGen`. The 2017 and 2018 MC samples are corrected separately. The distributions of PID variables before and after correction are shown in Figure 4 and Figure 5.

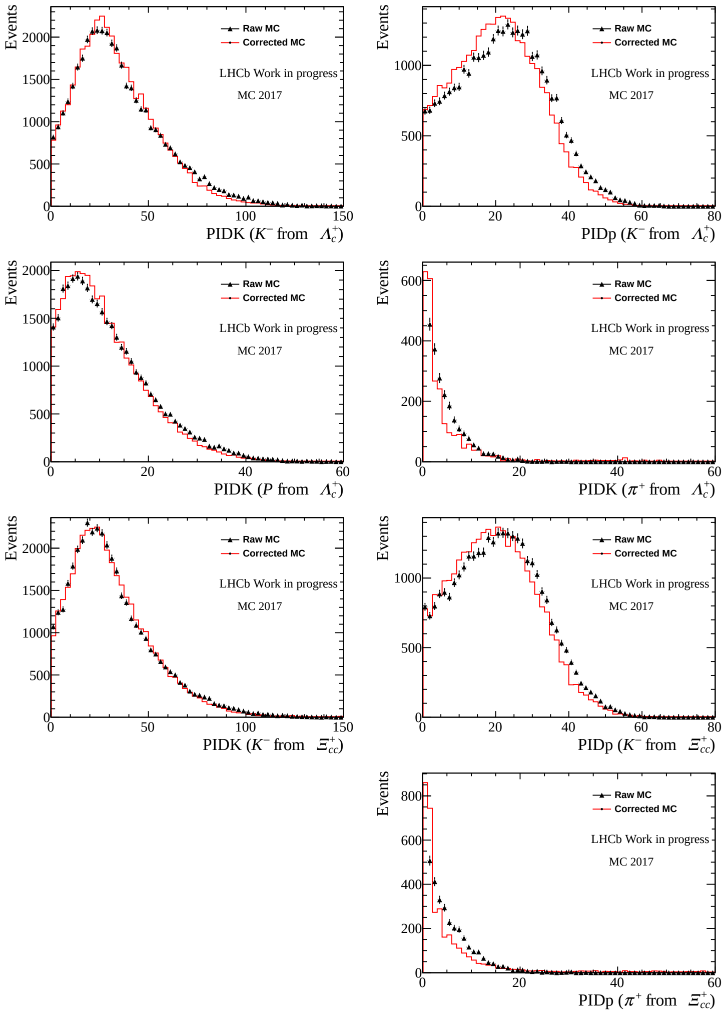

Figure 4: The distributions of PID variables before (black line) and after (red line) correction in 2017 MC samples.

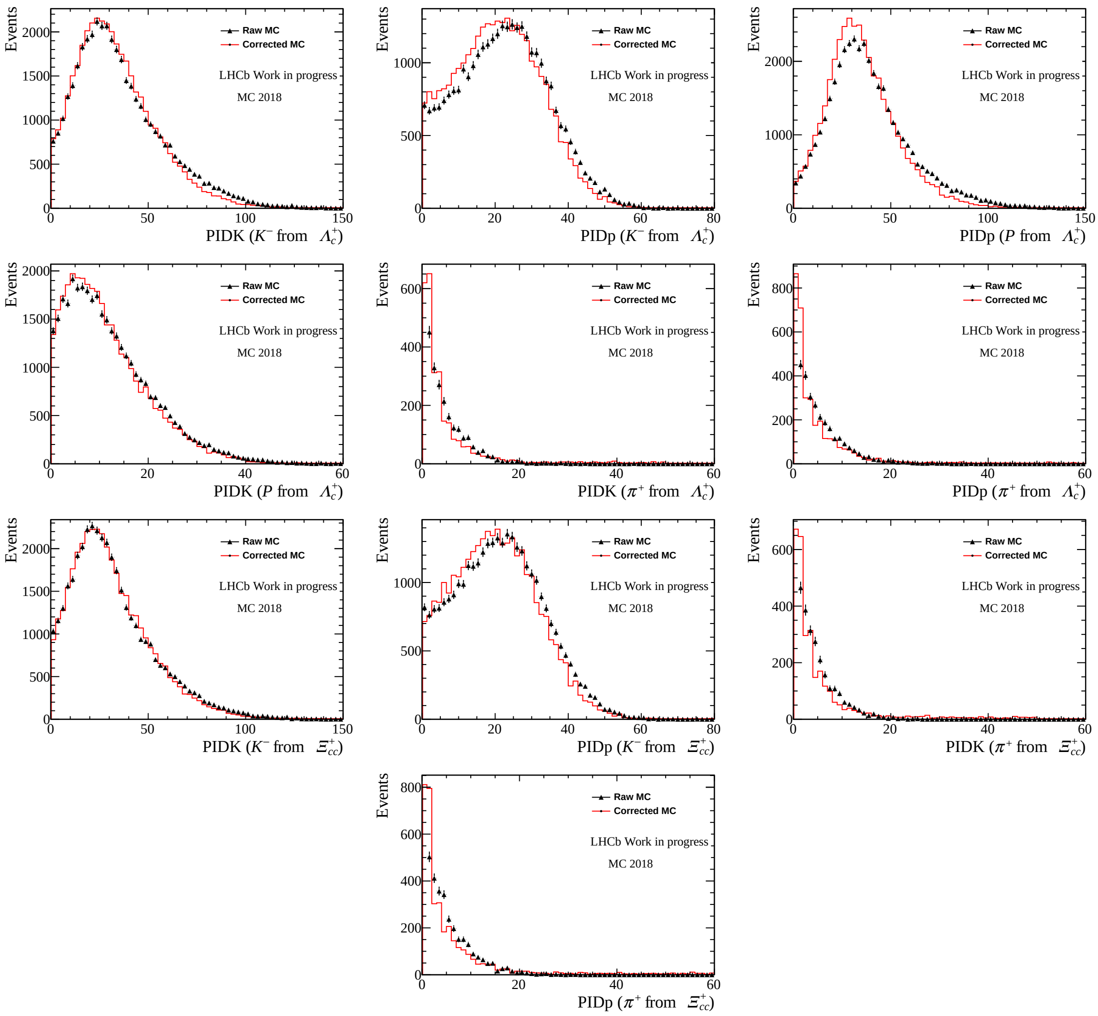

Figure 5: The distributions of PID variables before (black line) and after (red line) correction in 2018 MC samples.

4.2 Lifetime reweighting

Compared to the previous study, one of the main improvement is to do a lifetime re-weighting in MC samples. As shown in Table 2, the 2017 and 2018 MC samples are generated with the nominal mass hypothesis 3621.4 MeV/c^2 and lifetime configuration 80 fs. The lifetime is re-weighted in the 2017 and 2018 MC samples from 80 fs to 45 fs, aiming to improve the MVA training performance. The weight is defined as

$$w(t) = \frac{\frac{1}{\tau}\exp(-\frac{t}{\tau})}{\frac{1}{\tau_0}\exp(-\frac{t}{\tau_0})}, \tag{1}$$

where $\tau_0 = 80$ fs and $\tau = 45$ fs.

The MC samples are corrected and filtered before re-weighting. The Ξ_{cc}^+ decay time distribution before and after re-weighting is shown in Figure 6.

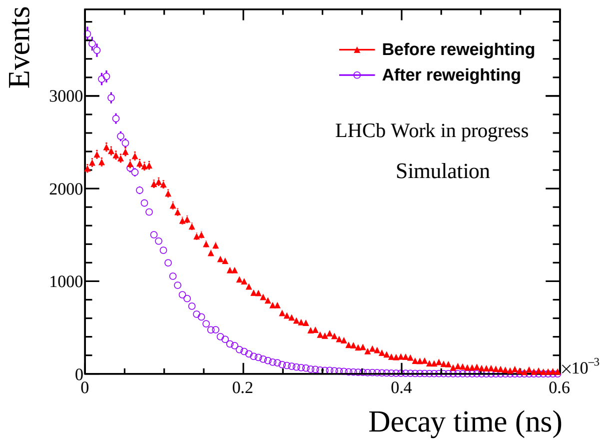

Figure 6: The Ξ_{cc}^+ decay time distribution before and after re-weighting.

4.3 Selection

The $\Xi_{cc}^{+} \to \Lambda_c^+ K^- \pi^+$ decay is selected in the following procedure.

- Events are filtered and candidates are reconstructed and selected centrally through the trigger.
- The K^- and π^+ are selected off-line and combined with inclusive Λ_c^+.
- A multivariate selection is applied.
- Clone and duplicated candidates are removed.

4.3.1 Trigger requirement

For 2016-2018 data, the Turbo output saves the candidates that were reconstructed at the trigger level and makes them available for offline analysis. The Ξ_{cc}^{+} baryon is reconstructed from the inclusive Λ_c^+ particles. The efficiency of this Turboline is studied in Table 3. The selection requirements are summarized in Table 3.

4.3.2 Offline reconstruction and pre-selection

The $\Xi_{cc}^{+} \to \Lambda_c^+ K^- \pi^+$ candidates are reconstructed from the Λ_c^+ candidates plus two tracks that pass appropriate hadron PID, track and p_{T} requirements. The three tracks are also required to form a vertex, with a χ^2 test cut. The reconstructed Ξ_{cc}^{+} candidates is required to come from the primary vertex, by imposing pointing requirements (DIRA and χ^2_{IP}). The selection is summarised in Table 4.

The Λ_c^+ invariant mass window is defined as $(2270\,\mathrm{MeV}/c^2, 2306\,\mathrm{MeV}/c^2)$. This is also included in the pre-selection, except which no other selections are required.

Table 3: Hlt2 trigger selections for Ξ_c^0.

Particle	Variable	Requirements
Λ_c^+ daughters	Track χ^2/ndf	< 3
	Momentum	$> 1\,\mathrm{GeV}/c$
	Transverse momentum	$> 0.2\,\mathrm{GeV}/c$
	Arithmetic sum of daughter p_{T}	$> 3\,\mathrm{GeV}/c$
	Maximum of daughter p_{T}	$> 1\,\mathrm{GeV}/c$
	Second maximum of daughter p_{T}	$> 0.4\,\mathrm{GeV}/c$
	χ^2_{IP} to PV	> 4
	Maximum of daughter χ^2_{IP}	> 16
	Second maximum of daughter χ^2_{IP}	> 9
	Proton particle ID DLL_{pp}	> 5
	Proton particle ID $\mathrm{DLL}_{pp} - \mathrm{DLL}_{pK}$	> 5
	Kaon particle ID DLL_{KK}	> 5
	Pion particle ID $\mathrm{DLL}_{K\pi}$	< 5
	Probability as a ghost track	< 0.4
Λ_c^+	Vertex χ^2_{vtx}/ndf	< 10
	Cosine of decay angle (DIRA)	> 0
	Decay time	$> 0.15\,\mathrm{ps}$
	Invariant mass $[\,\mathrm{MeV}/c^2\,]$	$(2201, 2553)$

Table 4: Offline selection for the $\Xi_{cc}^{+} \to \Lambda_c^{+} K^{-} \pi^{+}$ decay.

Particle	Variable	Cuts
Ξ_{cc}^{+} daughters	Ghost Probability	< 0.4
	Transverse momentum	$p_{\mathrm{T}}(\pi) > 0.15\,\mathrm{GeV}/c$
	Transverse momentum	$p_{\mathrm{T}}(K^{-}) > 0.2\,\mathrm{GeV}/c$
	K PID	ProbNNk > 0.1
	π PID	ProbNNpi > 0.2
Ξ_{cc}^{+}	Vector sum of daughter p_{T}	$> 2\,\mathrm{GeV}/c$
	Vertex quality	$\chi^2_{\mathrm{vtx}}/\mathrm{ndf} < 25$
	Impact parameter χ^2	$\chi^2_{\mathrm{IP}} < 25$
	Pointing angle	DIRA> 0.99

4.3.3 Multivariate selection

After the pre-selection, a multivariate analysis is then used to further improve the expected signal purity. The 2016 data and 2017, 2018 MC samples were used for the MVA studies, the result of which is then used to apply a MVA cut to 2016-2018 data. In the training, the simulated $\Xi_{cc}^{+} \to \Lambda_c^{+} K^{-} \pi^{+}$ events after the pre-selection are used as signals, WS data with the same pre-selection applied is used as backgrounds.

Due to the large sample size of the background, the WS data as background is reduced to include only the mass region 3610-3630 MeV/c^2 in the training and the testing. The standard TMVA approach spilt both the signal and background samples randomly into two equally sized disjoint subsamples, one for the training and the other for the testing.

The choice of the training variable initially follows the variable list from [9], then adding the corrected PID variables and applying the lifetime weight. The final 23 variables used for the training are listed in Table 5. The signal and background distribution of the variables are shown in Figure 7, while their correlation matrics are shown in Figure 8.

Table 5: The final 23 variables used for the MVA training, with the newly added variables marked.

	Variable	Number
	$\chi^2_{\mathrm{vtx}}/\mathrm{ndf}$ of the Λ_c^{+} vertex fit	1
	$\chi^2_{\mathrm{vtx}}/\mathrm{ndf}$ of the Ξ_{cc}^{+} vertex fit (without DTF)	1
	$\chi^2_{\mathrm{vtx}}/\mathrm{ndf}$ of the Ξ_{cc}^{+} candidate with PV constraint	1
	Log sized p_{T} of Ξ_{cc}^{+}, Λ_c^{+} and of their daughters	7
	$\cos^{-1}$(DIRA) of Ξ_{cc}^{+} to PV	1
	Log sized flight distance χ^2 of Λ_c^{+} to PV	1
	Log sized flight distance χ^2 of Λ_c^{+} to its original vertex	1
	Log sized flight distance χ^2 of Ξ_{cc}^{+} to PV	1
	Log sized χ^2_{IP} of daughters of Ξ_{cc}^{+} to PV	3
(new)	Momentum of proton from Λ_c^{+} to scalar sum of momenta of Λ_c^{+} daughters	1
(new)	Kaon particle ID DLL_{KK}	2
(new)	Pion particle ID $\mathrm{DLL}_{K\pi}$	2
(new)	Proton particle ID DLL_{pp}	1
	Total	23

From the conclusions of the previous study, the boosted decision tree (BDT) based MVA algorithms show the best performance. In total, five different BDT based algorithms are considered. The Receiver Operation Characteristics (ROC) curves are shown in Figure 9. The response distributions are shown in Figure 10. From the training results, BDTG algorithm is finally chosen for further study due to its best performance.

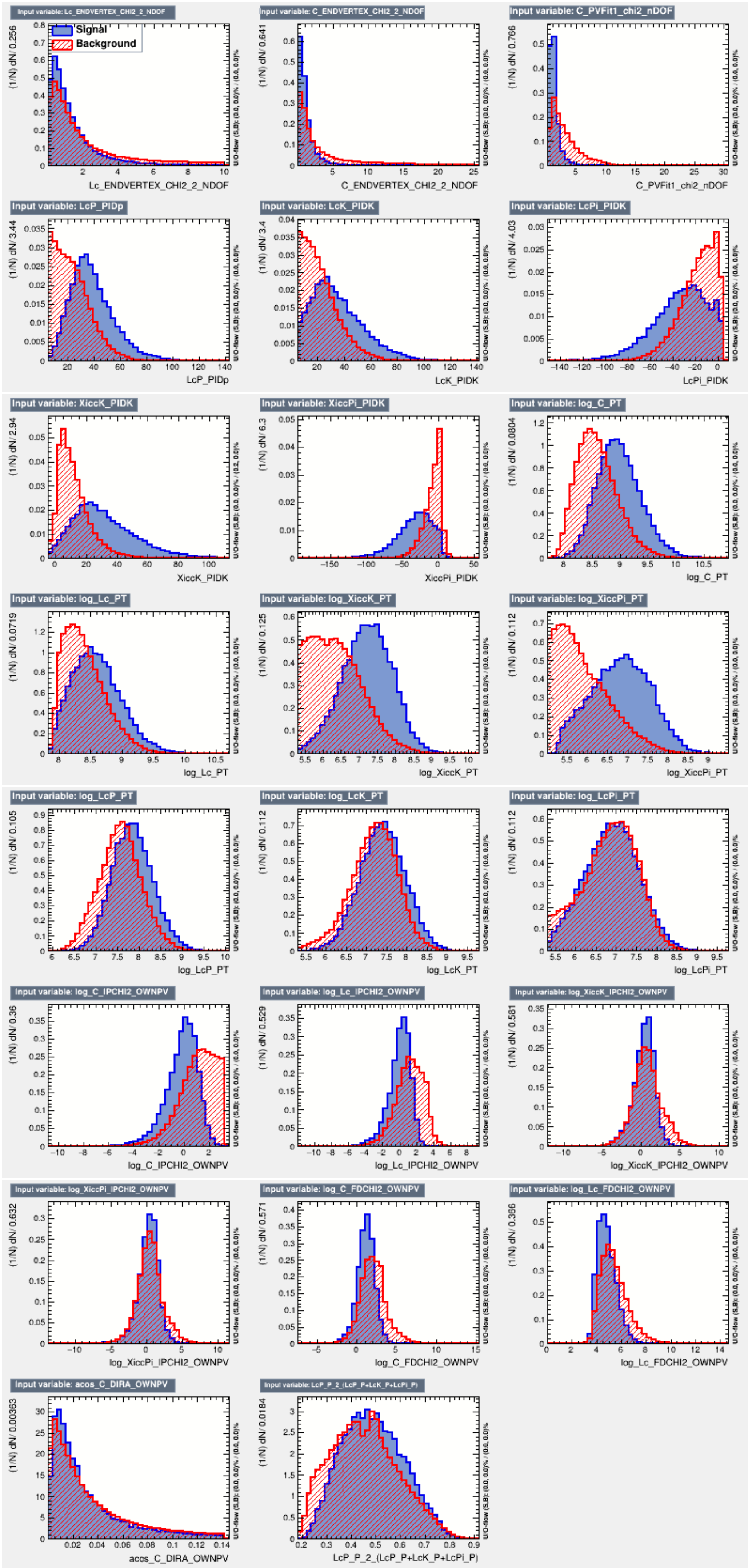

Figure 7: Distributions of input variables, compared between (blue) signals and (red) backgrounds.

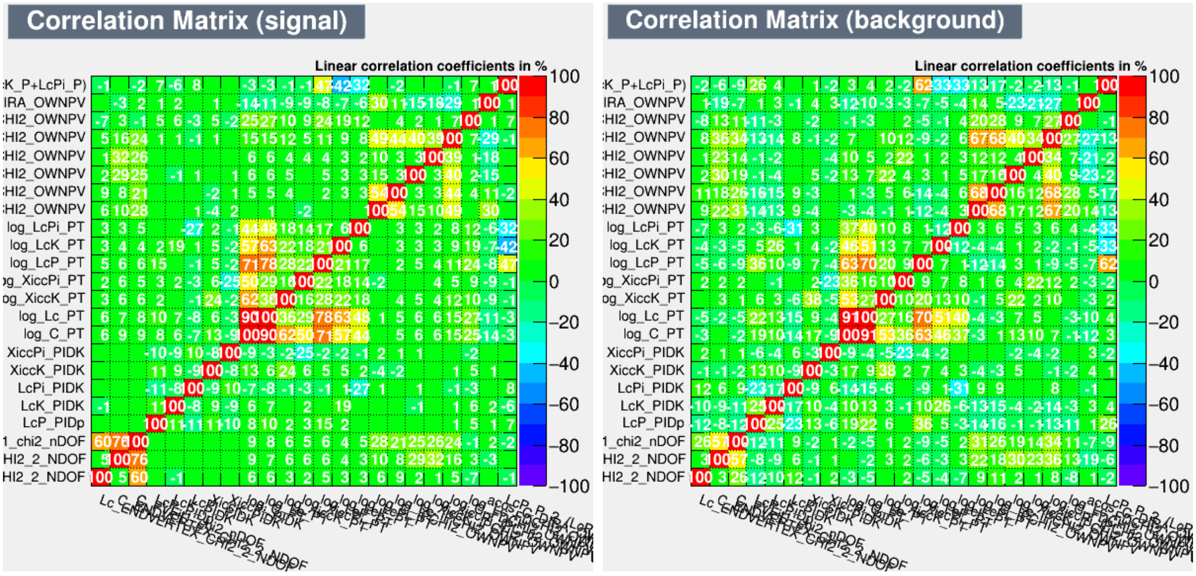

Figure 8: Correlation matrices for input variables used in MVA selectors, for (top) signal and (bottom) background.

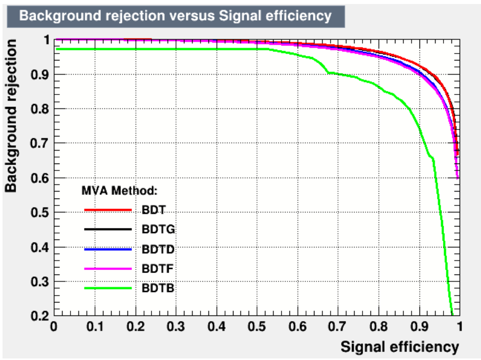

Figure 9: ROC curves for different BDT algorithms.

After obtaining the training result, the performance of the MVA algorithms is assessed quantitatively using the Punzi figure of merit (FoM). The FoM is an expression for the sensitivity of the search hypothesis, which is defined as

$$F(t) = \frac{\varepsilon(t)}{\frac{a}{2} + \sqrt{B(t)}}, \tag{2}$$

where $\varepsilon(t)$ is the total signal efficiency, $B(t)$ the expected background in the Ξ_{cc}^{+} signal window of the RS sample, and $a = 5$ the desired significance. The signal efficiency $\varepsilon(t)$ is calculated by

$$\varepsilon(t) = \frac{N_{\text{pass}}(t)}{N_{\text{gen}}},$$

where N_{gen} is the number of signals generated in the simulation and $N_{\text{pass}}(t)$ is the number of signals passing the Turbo selection, the preselection and the MVA cut t.

The optimal working point of a certain variable cut is the maximum point of FoM, which leads to the largest signal significance. The variation of $F(t)$ for BDTG algorithm is shown in Figure 11. The optimal working point is chosen as 0.989.

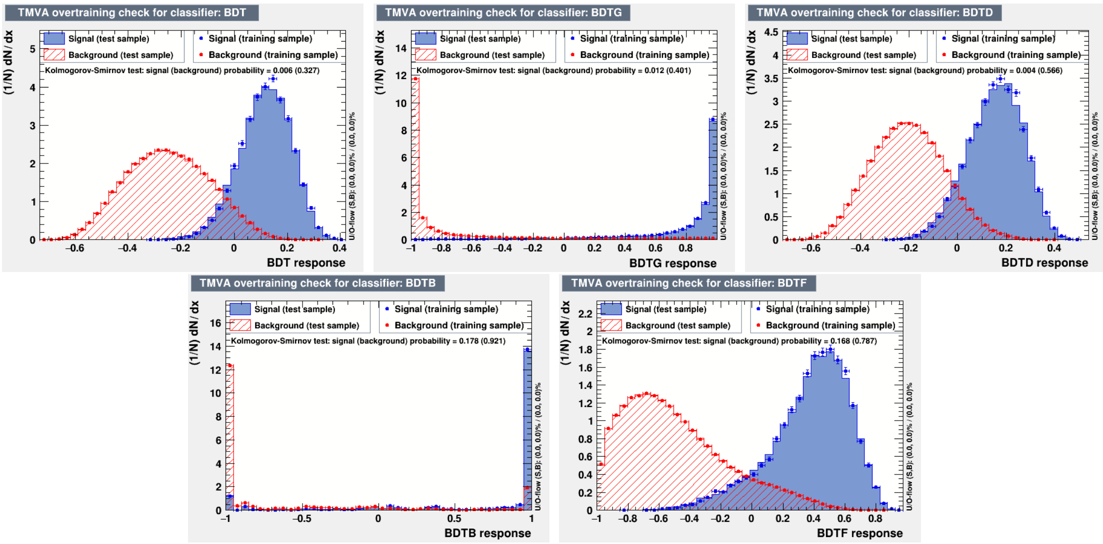

Figure 10: Response curves for BDT selectors: (top left) BDT, (top right) BDTG, (middle left) BDTD, (middle right) BDTB, (bottom) BDTF. The curves show the normalized MVA output distribution. The output for the training and testing samples are shown as points with error bars and as a shaded/hatched histogram, respectively.

After implementing the optimal BDTG working point selection, the Ξ_{cc}^{+} mass distribution with all selection is shown in Figure 12. The Λ_c^+ mass distribution is also checked in 2016-2018 RS data, showing a clean background in Figure 13.

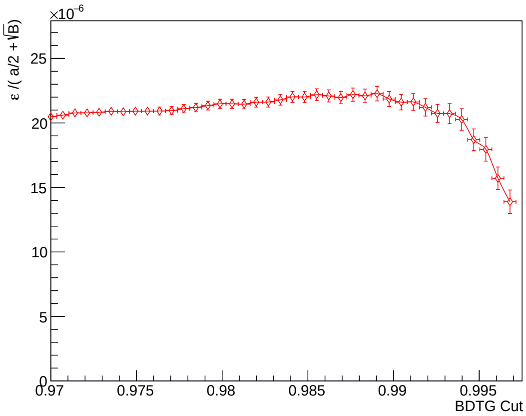

Figure 11: Punzi figure of merit $F(t)$ as a function of the BDTG cut t.

4.3.4 Removal of internal-track-clone candidates

An internal-track-clone candidate refers to the candidate in which at least one track is a clone of another track of the same candidate. As a multi-body decay with five final tracks, the reconstructed Ξ_{cc}^{+} candidates will suffer from the contamination of internal-track-clone candidates. The distribution of the angle between such two clone tracks $\delta\theta_{i,j}$ is supposed to peak at zero.

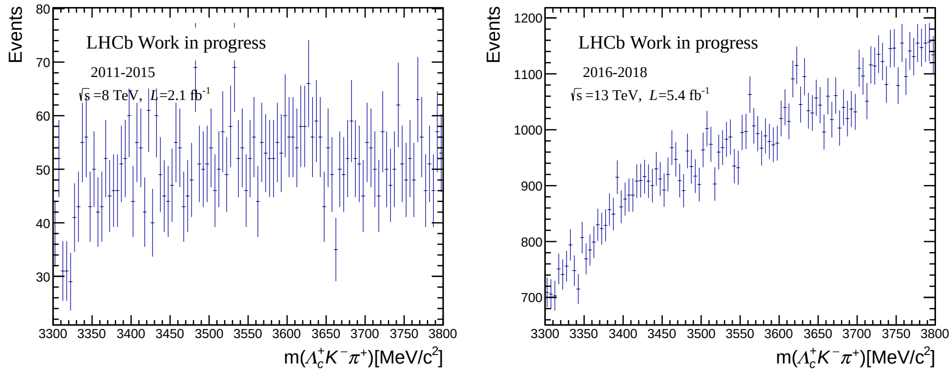

Figure 12: Ξ_{cc}^+ mass distribution of 2011-2015 data (left) 2016-2018 data (right) after the MVA cut.

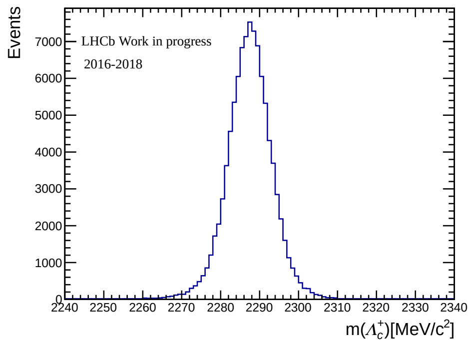

Figure 13: Λ_c^+ mass distribution after the MVA cut in 2016-2018 RS data.

A requirement of $\delta\theta_{i,j} > 0.5$ mrad is included in the selection sequence to remove the internal-track-clone candidates. This will remove around 3.0% candidates in the 2016 WS sample, while keeping $> 99\%$ of the signals in the MC sample.

4.3.5 Removal of duplicate candidates

Duplicate candidate is a special kind of multiple candidates, which may increase the signal significance artificially. In the $\Lambda_c^+(\to pK^-\pi^+)K^-\pi^+$ final states, there could be three scenarios:

- The K^- from the Λ_c^+ decay is swapped with the K^- directly from the Ξ_{cc}^+ decay;
- The π^+ from the Λ_c^+ decay is swapped with the π^+ directly from the Ξ_{cc}^+ decay;
- Combination of the above two cases.

Such candidates are removed in the data by comparing the track ID and requiring every candidate contains at least one track not identical to other candidates of the same event. Table 6 summarizes the removed candidates in 2016-2018 data.

Table 6: Yields and number of removed clone and duplicated candidates in 2016-2018 data after all the selections.

Year	Yields before removal	Removed clone	Removed duplication	Yields after removal
2016	21786	-27	-50	21709 (99.64%)
2017	33235	-191	-23	33021 (99.36%)
2018	41859	-88	-98	41673 (99.56%)

4.4 Mass measurement

In this section, the initial steps of the measurement of the Ξ_{cc}^{+} invariant mass is briefly introduced.

4.4.1 Fit model

For the signal events, the invariant mass distribution shape is studied with MC samples. As a decay process, this distribution is expected to be well described by the one-sided Crystal Ball Function (CB), which is defined as

$$f(x;\alpha,N,\bar{x},\sigma)=\begin{cases} e^{-\frac{1}{2}(\frac{x-\bar{x}}{\sigma})^2} & \text{for } \frac{x-\bar{x}}{\sigma}>-\alpha \\ \left(\frac{N}{|\alpha|}\right)^N e^{-\frac{|\alpha|^2}{2}}\left(\frac{N}{|\alpha|}-|\alpha|-\frac{x-\bar{x}}{\sigma}\right) & \text{for } \frac{x-\bar{x}}{\sigma}\leq-\alpha \end{cases} \tag{3}$$

One of the two correlated parameters N and α is fixed to avoid uncertainty. Here we choose $N=1$. To consider the resolution of the momentum measurement, the signal is fitted with two CB functions, correlated linearly with a scale factor f:

$$\mathrm{f}\cdot\mathrm{PDF}_1+(1-\mathrm{f})\cdot\mathrm{PDF}_2 \tag{4}$$

The fitted signal distribution is shown in Figure 14, with the optimal fitting results and uncertainties.

The Ξ_{cc}^{+} mass is measured from the invariant mass distribution of $\Lambda_c^+K^-\pi^+$ fitted with signal plus combinatorial background components. To correct the measurement bias caused by Λ_c^+ mass, the difference $DM\equiv M(\Xi_{cc}^{+})-M(\Lambda_c^+)+M_{PDG}(\Lambda_c^+)$ is used, where $M(\Xi_{cc}^{+})$ and $M(\Lambda_c^+)$ are values observed applying DTF.

The invariant mass distribution in data for events passing all the event selections is shown in Figure 15. The parameters of the signal pdf is fixed to the optimal fitting result from MC signal samples in Figure 14, while The mean value μ is allowed to float in the signal mass region, with an initial value of $3622.7\,\mathrm{MeV}/c^2$. Besides, the background shape is fitted with Chebyshev Polynomial up to the second order. Due to the large background events number, the mass distribution is fitted roughly in a binned data set, whose bin width is $1\,\mathrm{MeV}/c^2$.

4.4.2 Local significance

Without considering any systematics, the local p-value is calculated using the one-sided Gaussian tail convention, by

$$\texttt{0.5*TMath::Prob}(2\Delta\ln L,\texttt{1}) \tag{5}$$

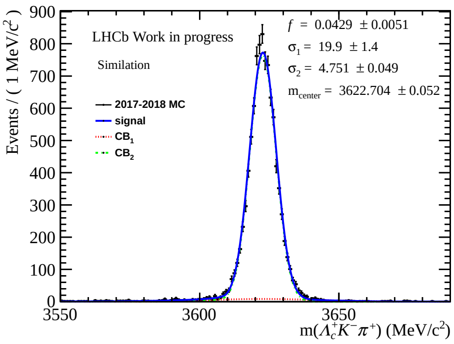

Figure 14: Ξ_{cc}^{+} mass distribution of the MC sample, fitted with two CB functions. The optimal fitting result is marked on the figure.

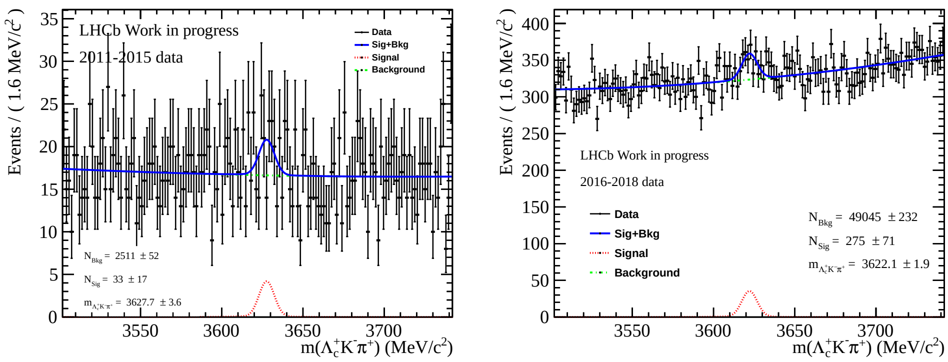

Figure 15: Fitting the invariant mass of Ξ_{cc}^{+} in 2011-2015 data (left) and 2016-2018 data (right).

as a function of $m(\Xi_{cc}^{+})$ for Run1, Run2, and total data sets, as shown in Figure 16. To reduce the influence of the marginal effect, the mass is fitted in the symmetric $\pm 120\,\mathrm{MeV}/c^2$ region of the fixed hypothetical mass mean value μ. From the scanning result, the local p-value reaches 4.47 σ at $3622\,\mathrm{MeV}/c^2$, which shows a 7% improvement comparing with the previous combined result (4.2 σ).

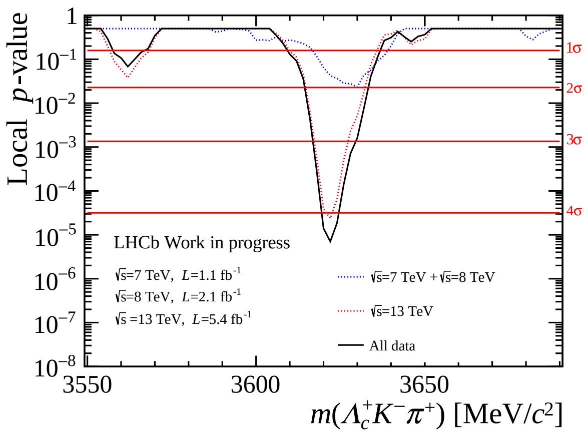

Figure 16: The Local p-value as a function of m(Ξ_{cc}^{+}) for the combined Run1 and Run2 data sets with the MVA selection optimised for lifetime hypothesis $\tau = 45\,\mathrm{fs}$.

5 Search in $\Xi_{cc}^{+} \to \Xi_{c}^{0}\pi^{+}$

5.1 PID correction

In order to enhance the similarity between the MC simulation samples and the real data, MC samples are corrected based on PID calibration data, using the PID resampling tool `PIDGen`. The 2017 and 2018 MC samples are corrected separately. The distributions of PID variables before and after correction are shown in Figure 17 and Figure 18.

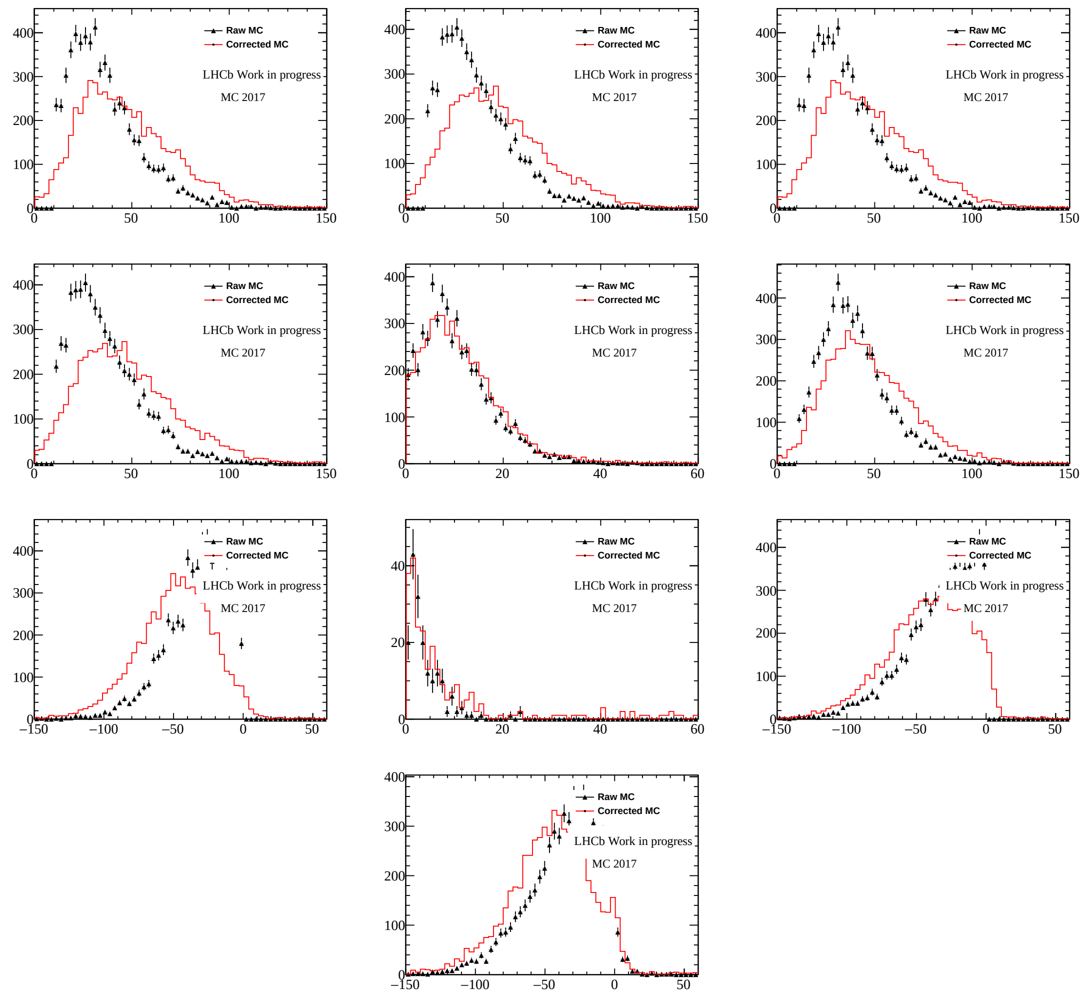

Figure 17: The distributions of PID variables before (black line) and after (red line) correction in 2017 MC samples.

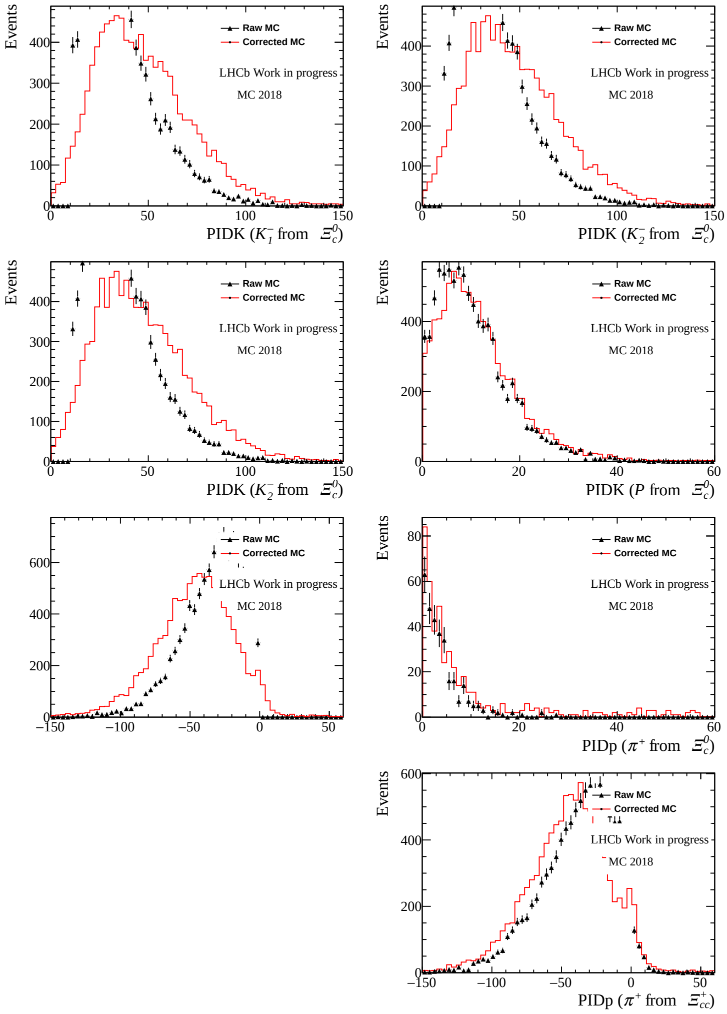

Figure 18: The distributions of PID variables before (black line) and after (red line) correction in 2018 MC samples.

5.2 Lifetime reweighting

Ξ_{cc}^{+} lifetime in the 2017 and 2018 MC samples are similarly re-weighted from 80 fs to 45 fs, aiming to improve the MVA training performance.

The MC samples are corrected and filtered before re-weighting. The Ξ_{cc}^{+} decay time distribution before and after re-weighting is shown in Figure 19.

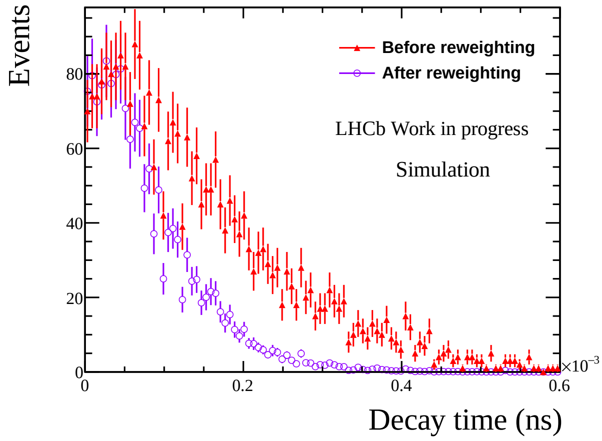

Figure 19: The Ξ_{cc}^{+} decay time distribution before and after re-weighting.

5.3 Selection

The $\Xi_{cc}^{+} \to \Xi_{c}^{0}\pi^{+}$ decay is selected in the following procedure.

- Events are filtered and candidates are reconstructed and selected centrally through the trigger.
- The π^{+} are selected off-line and combined with inclusive Ξ_{c}^{0}.
- A multivariate selection is applied.

5.3.1 Trigger requirement

For 2016-2018 data, the Turbo output saves the candidates that were reconstructed at the trigger level and makes them available for offline analysis. The Ξ_{cc}^{+} baryon is reconstructed from the inclusive Ξ_{c}^{0} particles. The selection efficiency of this Turboline is studied in Table 7. The selection shows a rather low efficiency of Ξ_{c}^{0}, which could be improved in Run3.

5.3.2 Offline reconstruction and pre-selection

The Ξ_{cc}^{+} candidates are reconstructed from the Ξ_{c}^{0} candidates plus one track that passes appropriate hadron PID, track and p_{T} requirements. The two tracks are also required to form a vertex, with a χ^2 test cut. The reconstructed Ξ_{cc}^{+} candidates is required to come from the primary vertex, by imposing pointing requirements (DIRA and χ^2_{IP}).

Table 7: Hlt2 trigger selection efficiency.

Particle	**Cut**	N_{events}	**efficiency**
Ξ_{c}^{0} daughters	Proton $P_T > 500.0$	398922	$(98.03 \pm 0.02)\%$
	Kaon 1 $P_T > 500.0$	348296	$(87.31 \pm 0.05)\%$
	Kaon 2 $P_T > 500.0$	310137	$(89.04 \pm 0.05)\%$
	Pion $P_T > 500.0$	182099	$(58.72 \pm 0.09)\%$
	Proton χ^2_{IP} to PV> 4.0	53772	$(29.53 \pm 0.11)\%$
	Kaon 1 χ^2_{IP} to PV> 4.0	20126	$(37.43 \pm 0.21)\%$
	Kaon 2 χ^2_{IP} to PV> 4.0	9226	$(45.84 \pm 0.35)\%$
	Pion χ^2_{IP} to PV> 4.0	5076	$(55.02 \pm 0.52)\%$
Ξ_{c}^{0}	$\chi^2_{\mathrm{IP}}/ndf < 10.0$	4553	$(89.70 \pm 0.43)\%$
	$DIRA > cos(0.01)$	3179	$(69.82 \pm 0.68)\%$
	Flight distance $\chi^2 > 10.0$	3158	$(99.34 \pm 0.14)\%$
	Lifetime > 0.0001	2912	$(92.21 \pm 0.48)\%$
	Invariant mass $\in (2386.0, 2780)$	2908	$(99.86 \pm 0.07)\%$
	Arithmetic sum of daughter $P_T > 3000.0$	2904	$(99.86 \pm 0.07)\%$
	At least one of the daughter particles $P_T > 1000$	2898	$(99.79 \pm 0.08)\%$
	At least two of the daughter particles $P_T > 500$	2898	$(100.00 \pm 0.00)\%$
	At least one of the daughter particles χ^2_{IP} to PV> 8.0	2800	$(96.62 \pm 0.34)\%$
	At least two of the daughter particles χ^2_{IP} to PV> 6.0	2701	$(96.46 \pm 0.35)\%$
Ξ_{cc}^{+}	$\chi^2_{\mathrm{IP}}/ndf < 20.0$	2664	$(98.63 \pm 0.22)\%$
	DIRA $> cos(1.57079632679)$	2344	$(87.99 \pm 0.63)\%$
	Invariant mass $\in (3100, 4000)$	2343	$(99.96 \pm 0.04)\%$
	Arithmetic sum of Ξ_{c}^{0} and π^{+} $P_T > 2000.0$	2343	$(100.00 \pm 0.00)\%$

5.3.3 Multivariate selection

After the pre-selection, a multivariate analysis is then used to further improve the expected signal purity. The 2016 data and 2016-2018 MC samples were used for the MVA studies, the result of which is then used to apply a MVA cut to 2016-2018 data. In the training, the simulated $\Xi_{cc}^{+} \to \Lambda_c^{+} K^{-} \pi^{+}$ events after the pre-selection are used as signals, WS data with the same pre-selection applied is used as backgrounds.

The final 25 variables used for the training are listed in Table 8. The signal and background distribution of the variables are shown in Figure 20, while their correlation matrics are shown in Figure 21.

Table 8: The final 23 variables used for the MVA training, with the newly added variables marked.

Category	Variable	Number
Fit quality	$\chi^2_{\rm vtx}$/ndf of the Ξ_c^0 vertex fit	1
	$\chi^2_{\rm vtx}$/ndf of the Ξ_{cc}^+ vertex fit (without DTF)	1
	$\chi^2_{\rm vtx}$/ndf of the Ξ_{cc}^+ candidate with PV constraint	1
Topology	$\cos^{-1}$(DIRA) of Ξ_{cc}^+ to PV	1
	Log sized flight distance χ^2 of Ξ_c^0 to PV	1
	Log sized flight distance χ^2 of Ξ_c^0 to its original vertex	1
	Log sized flight distance χ^2 of Ξ_{cc}^+ to PV	1
	Log sized χ^2_{IP} of daughters of Ξ_{cc}^+ to PV	3
	Log sized sum of χ^2_{IP} of Ξ_{cc}^+ daughters to PV	1
Kinematics	Log sized p_T of Ξ_{cc}^+, Ξ_c^0 and of their daughters	7
	Log sized sum of p_T of Ξ_{cc}^+ daughters	1
	Momentum of proton from Ξ_c^0 / scalar sum of Ξ_c^0 daughters momenta	1
PID	Kaon particle ID DLL$_{KK}$	2
	Pion particle ID DLL$_{K\pi}$	2
	Proton particle ID DLL$_{pp}$	1
Total		25

From the conclusions of the previous study, the boosted decision tree (BDT) based MVA algorithms show the best performance. In total, five different BDT based algorithms are considered. The ROC curves are shown in Figure 22. The response distributions are shown in Figure 23. From the training results, BDT algorithm is finally chosen for further study due to its best performance.

The FoM is used to determine the optimal working point of BDT algorithm. The optimal working point of a certain variable cut is the maximum point of FoM, which leads to the largest signal significance. The variation of $F(t)$ for BDTG algorithm is shown in Figure 24. The optimal working point is chosen as 0.24.

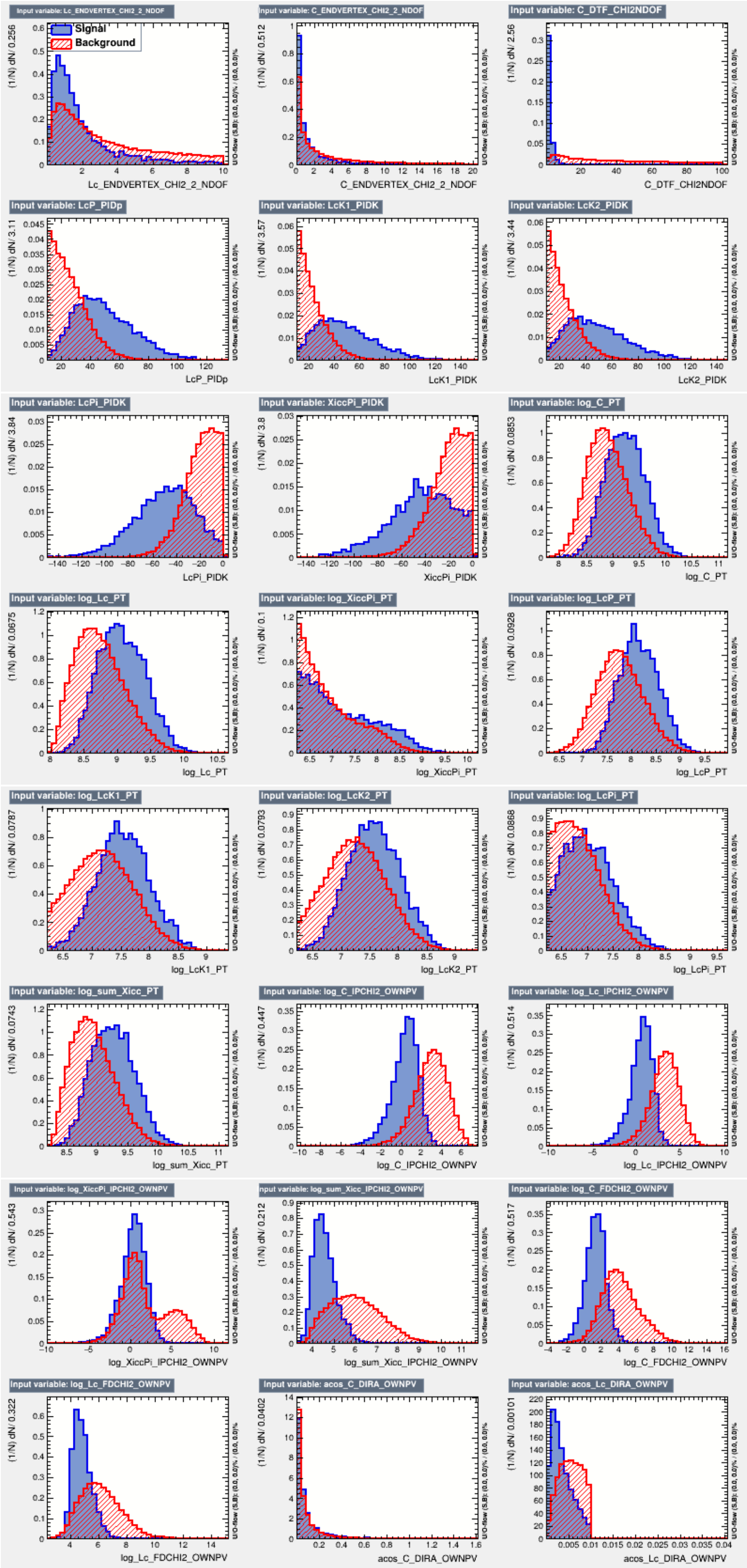
Input variable: Lc_ENDVERTEX_CHI2_2_NDOF
Signal
Background
Input variable: C_ENDVERTEX_CHI2_2_NDOF
Input variable: C_DTF_CHI2NDOF
Input variable: LcP_PIDp
Input variable: LcK1_PIDK
Input variable: LcK2_PIDK
Input variable: LcPi_PIDK
Input variable: XiccPi_PIDK
Input variable: log_C_PT
Input variable: log_Lc_PT
Input variable: log_XiccPi_PT
Input variable: log_LcP_PT
Input variable: log_LcK1_PT
Input variable: log_LcK2_PT
Input variable: log_LcPi_PT
Input variable: log_sum_Xicc_PT
Input variable: log_C_IPCHI2_OWNPV
Input variable: log_Lc_IPCHI2_OWNPV
Input variable: log_XiccPi_IPCHI2_OWNPV
Input variable: log_sum_Xicc_IPCHI2_OWNPV
Input variable: log_C_FDCHI2_OWNPV
Input variable: log_Lc_FDCHI2_OWNPV
Input variable: acos_C_DIRA_OWNPV
Input variable: acos_Lc_DIRA_OWNPV
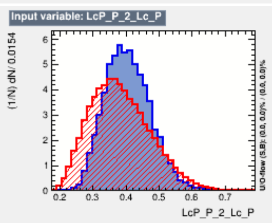
Input variable: LcP_P_2_Lc_P
LcP_P_2_Lc_P

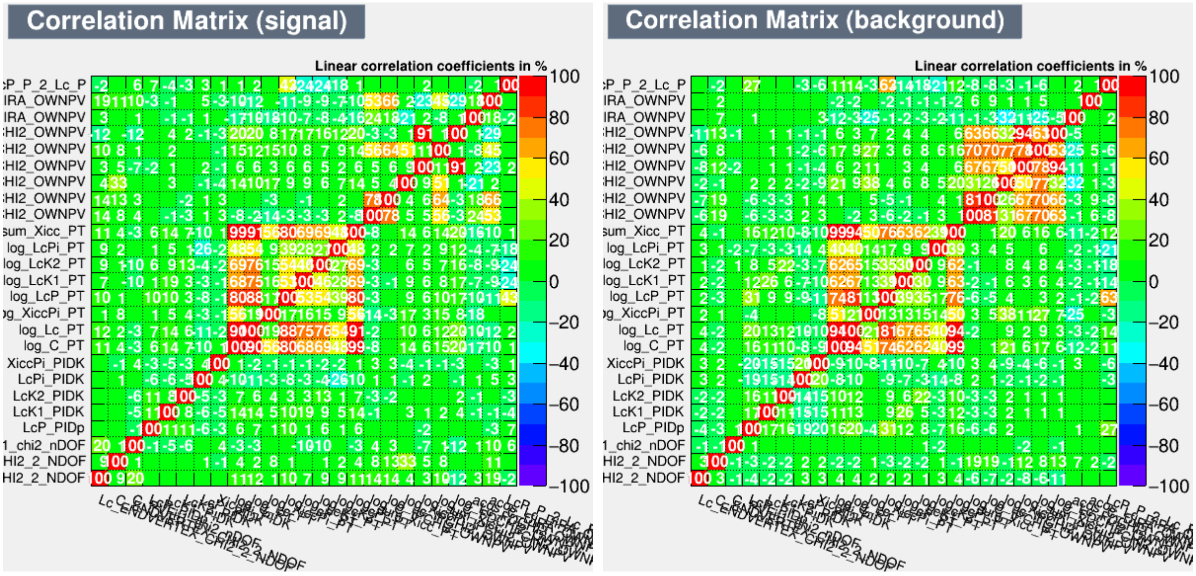

Figure 21: Correlation matrices for input variables used in MVA selectors, for (top) signal and (bottom) background.

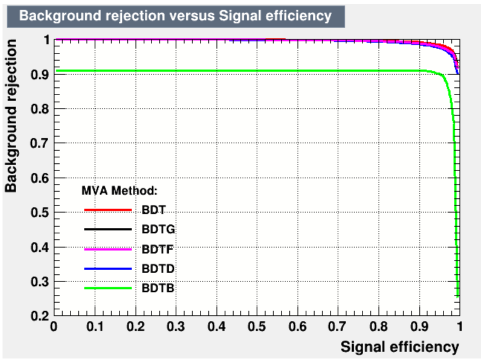

Figure 22: ROC curves for different BDT algorithms.

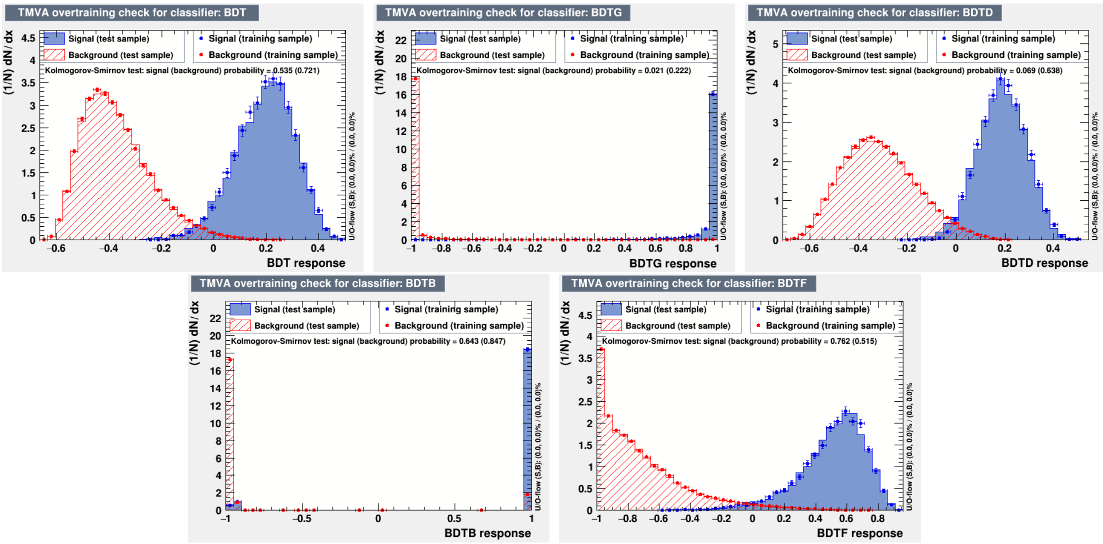

Figure 23: Response curves for BDT selectors: (top left) BDT, (top right) BDTG, (middle left) BDTD, (middle right) BDTB, (bottom) BDTF. The curves show the normalized MVA output distribution. The output for the training and testing samples are shown as points with error bars and as a shaded/hatched histogram, respectively.

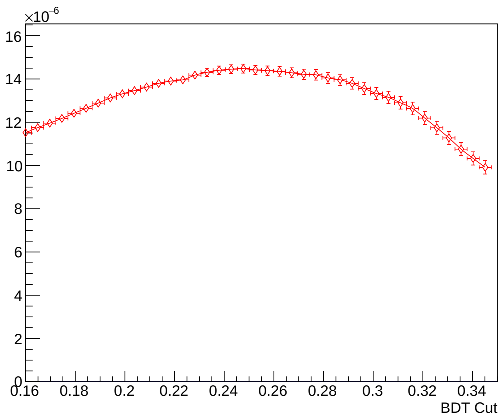

Figure 24: Punzi figure of merit $F(t)$ as a function of the BDT cut t.

5.4 Mass distribution

After applying all the selections, the mass distribution of Ξ_c^0 in Figure 25 is very clean. Also, the mass distribution of Ξ_{cc}^+ candidates in the central signal region is shown in Figure 26, where the WS data is scaled to RS according to the number of events in the upper sideband region $[3800, 4000]$ MeV/c^2. There is no fake peak structure in WS data.

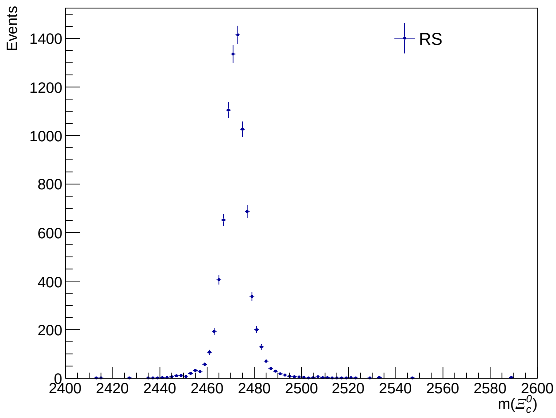

Figure 25: Ξ_c^0 mass distribution after applying all selections.

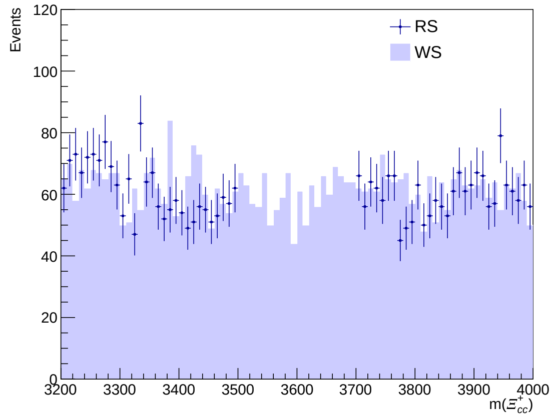

Figure 26: The mass distribution of Ξ_{cc}^+ candidates, where the WS data is scaled to RS according to $\mathrm{N_{events}}$ in $[3800, 4000]$ MeV/c^2. The shaded area repredents the WS events.

The lower sideband of Ξ_{cc}^+ mass spectrum is also checked. The WS data is scaled to RS according to the number of events in the mass region $[3200, 3500]$ MeV/c^2. The selection is relaxed to $p_{\mathrm{T}} > 200$ MeV/c and BDT cut > 0.15. We can see clear signal of excited Ξ_{c}^+ states at 2645 and 2790 MeV/c^2, even though the selection is not optimal for prompt signals. There are some possible signals of excited Ξ_c^+ around 2900 MeV/c^2, which will be further studied in Section 5.5.

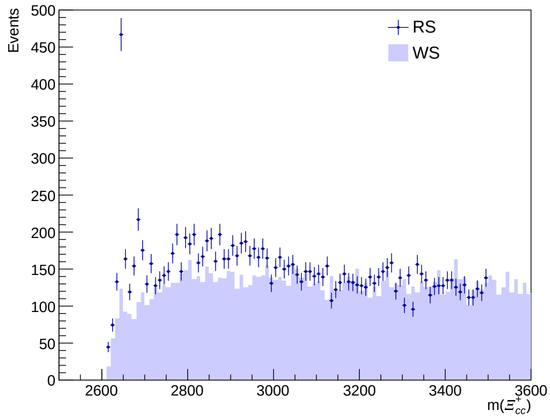

Figure 27: The mass distribution of Ξ_{cc}^{+} candidates in lower sideband region, where the WS data is scaled to RS according to $\mathrm{N_{events}}$ in $[3200, 3500]$ $\mathrm{MeV/c^2}$. The shaded area repredents the WS events.

5.5 Search for excited Ξ_c^+ states

The excited Ξ_c^+ states are searched in $\Xi_c^+ \to \Xi_c^0 \pi^+$ decay. In order to select the prompt signals, the Ξ_c^0 signal is studied and its selection is optimized.

5.5.1 Selection of Ξ_c^0

The Ξ_c^0 mass distribution in $\Xi_c^0 \to pK^-K^-\pi^+$ decay in 2016 cut-based RS data is fitted with two Gaussian for signal and a straight line for background, which is shown in Figure 28.

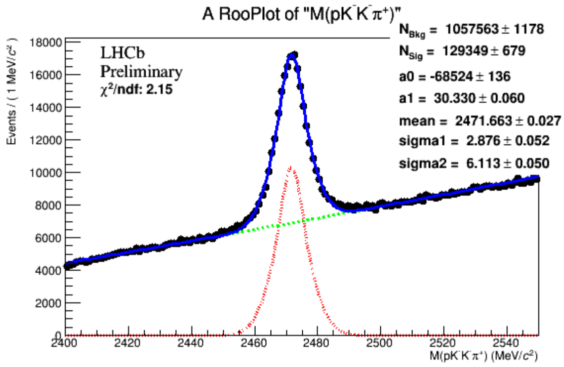

Figure 28: The fitting result of the mass distribution of Ξ_c^0 in RS data.

Next, the signal and background are separated using the SPlot method. And then they are used for MVA training with signal and background weights. The BDT method was chosen, and the response curve is shown in Figure 29.

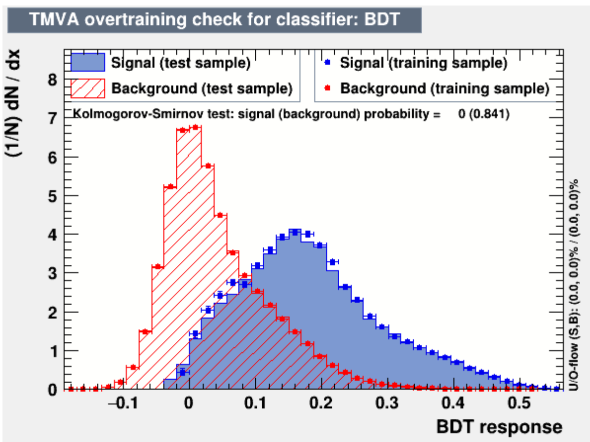

Figure 29: Response curve for BDT selector.

The BDT performance is checked in Figure 30. The blue line shows the Ξ_c^0 mass distribution after BDT cut > 0.1 and the red line is the events removed after the same cut.

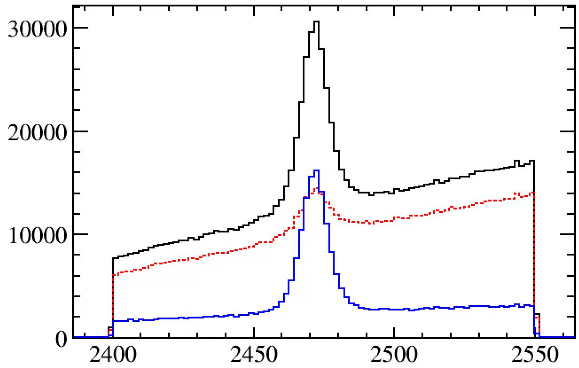

Figure 30: Ξ_c^0 mass distribution (black line). The blue line shows the Ξ_c^0 mass distribution after BDT cut > 0.1 and the red line is the events removed after the same cut.

5.5.2 $\Xi_c^0\pi^+$ mass spectrum

The $\Xi_c^0\pi^+$ is reconstructed with the Ξ_c^0 selected in Section 5.5.1 and an off-line selected π^+. The mass spectrum is shown in Figure 31. The 2645 MeV/c^2 excited state of Ξ_c^+ is clearly shown in the figure. And the possible excited Ξ_c^+ states are marked red. The $\Omega_c^0\pi^+$ mass spectrum is also studied in the same way. The result is shown in Figure 32.

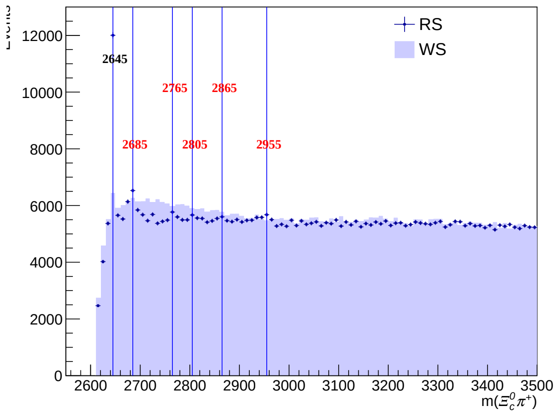

Figure 31: $\Xi_c^0\pi^+$ mass spectrum, with possible excited Ξ_c^+ states marked red.

So far, it is only a very preliminary study of the Ξ_c^+ excited states. Further study is still needed and will be conducted in the future.

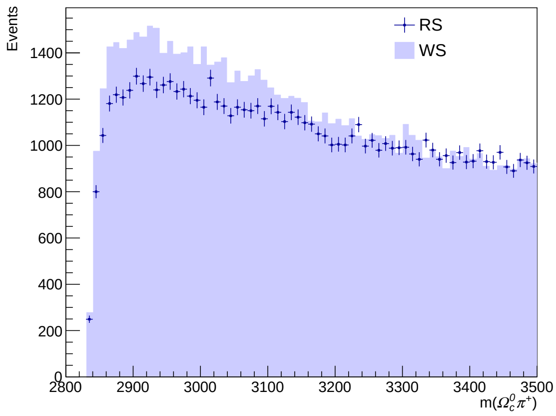

Figure 32: $\Omega_c^0\pi^+$ mass spectrum.

6 Conclusion

The re-optimization of the search for Ξ_{cc}^{+} in $\Xi_{cc}^{+} \to \Lambda_c^{+} K^{-} \pi^{+}$ decay is performed using Run1 and Run2 data. The local significance is improved to 4.5 σ. A preliminary study of the event selection and background in the new decay mode $\Xi_{cc}^{+} \to \Xi_c^{0} \pi^{+}$ is performed using Run2 data. Finally, the possible excited Ξ_c^{+}, Ω_c^{0} states are checked in the $\Xi_c^{0} \pi^{+}$ and $\Omega_c^{0} \pi^{+}$ mass spectrum.

References

[1] A. V. Berezhnoy, V. V. Kiselev, A. K. Likhoded, and A. I. Onishchenko, *Doubly charmed baryon production in hadronic experiments*, Phys. Rev. **D57** (1998) 4385, `arXiv:hep-ph/9710339`.

[2] K. Anikeev *et al.*, *B physics at the Tevatron: Run II and beyond,* in *Workshop on B physics at the Tevatron: Run II and beyond, Batavia, Illinois, September 23-25, 1999*, 2001. `arXiv:hep-ph/0201071`.

[3] C.-H. Chang, C.-F. Qiao, J.-X. Wang, and X.-G. Wu, *Estimate of the hadronic production of the doubly charmed baryon Ξ_{cc} in the general-mass variable-flavor-number scheme*, Phys. Rev. **D73** (2006) 094022, `arXiv:hep-ph/0601032`.

[4] C.-H. Chang, J.-P. Ma, C.-F. Qiao, and X.-G. Wu, *Hadronic production of the doubly charmed baryon Ξ_{cc} with intrinsic charm*, J. Phys. **G34** (2007) 845, `arXiv:hep-ph/0610205`.

[5] LHCb collaboration, R. Aaij *et al.*, *Observation of the doubly charmed baryon Ξ_{cc}^{++}*, Phys. Rev. Lett. **119** (2017) 112001, `arXiv:1707.01621`.

[6] SELEX collaboration, A. Ocherashvili *et al.*, *Confirmation of the double charm baryon $\Xi_{cc}^{+}(3520)$ via its decay to pD^+K^-*, Phys. Lett. **B628** (2005) 18, `arXiv:hep-ex/0406033`.

[7] LHCb collaboration, R. Aaij *et al.*, *First observation of the doubly charmed baryon decay $\Xi_{cc}^{++} \to \Xi_c^+\pi^+$*, Phys. Rev. Lett. **121** (2018) 162002, `arXiv:1807.01919`.

[8] LHCb collaboration, R. Aaij *et al.*, *Measurement of the lifetime of the doubly charmed baryon Ξ_{cc}^{++}*, Phys. Rev. Lett. **121** (2018) 052002, `arXiv:1806.02744`.

[9] LHCb collaboration, R. Aaij *et al.*, *Search for the doubly charmed baryon Ξ_{cc}^{+}*, Sci. China Phys. Mech. Astron. **63** (2020) 221062, `arXiv:1909.12273`.

[10] LHCb collaboration, R. Aaij *et al.*, *Search for the doubly charmed baryon Ξ_{cc}^{+} in the $\Xi_c^+\pi^-\pi^+$ final state,* LHCb-PAPER-2021-019, in preparation.

[11] BABAR Collaboration, B. Aubert *et al.*, *Search for doubly charmed baryons Ξ_{cc}^{+} and Ξ_{cc}^{++} in babar*, Phys. Rev. D **74** (2006) 011103.

[12] Belle Collaboration, Y. Kato *et al.*, *Search for doubly charmed baryons and study of charmed strange baryons at belle*, Phys. Rev. D **89** (2014) 052003.

[13] F.-S. Yu *et al.*, *Discovery potentials of doubly charmed baryons*, Chinese Physics C **42** (2018) 051001.

[14] C.-H. Chang, J.-X. Wang, and X.-G. Wu, *GENXICC: a generator for hadronic production of the double heavy baryons Ξ_{cc}, Ξ_{bc} and Ξ_{bb}*, Comput. Phys. Commun. **177** (2007) 467, `arXiv:hep-ph/0702054`; C.-H. Chang, J.-X. Wang, and X.-G. Wu, *GENXICC2.0: an upgraded version of the generator for hadronic production of double heavy baryons Ξ_{cc}, Ξ_{bc} and Ξ_{bb}*, Comput. Phys. Commun. **181** (2010) 1144, `arXiv:0910.4462`.